J. Fluid Mech. (1994), vol. 275, pp. 379–405

Low-dimensional bifurcation phenomena in Taylor–Couette flow with discrete azimuthal symmetry

By J. J. KOBINE† AND T. MULLIN

Atmospheric, Oceanic and Planetary Physics, Clarendon Laboratory, University of Oxford, Parks Road, Oxford, OX1 3PU, UK

(Received 30 November 1993 and in revised form 19 April 1994)

We report the results of an experimental study of flow in a Taylor–Couette system where the usual circular outer cylinder is replaced by one with a square cross-section. The objective is to determine the validity of low-dimensional dynamical systems as a descriptive framework for flows in a domain without the special continuous symmetry of the original problem. We focus on a restricted version of the flow, where the steady flow consists of a single cell, thereby minimizing the multiplicity of solutions. The steady-state bifurcation structure is found to be qualitatively unchanged from that of the standard system. A complex but self-consistent bifurcation structure is uncovered for time-dependent flows, culminating in observations of dynamics similar to those of the finite-dimensional Šil'nikov mechanism. Such behaviour has been observed in the standard system with continuous azimuthal symmetry. The present results extend the range of closed-flow problems where there is an apparent connection between the infinite-dimensional Navier–Stokes equations and finite-dimensional dynamical systems.

1. Introduction

There has recently been much progress in understanding certain complicated fluid flow phenomena by using ideas which originate from the study of low-dimensional nonlinear dynamical models. Examples have been found of transitions from regular to irregular flow behaviour which occur by means of simple deterministic mechanisms. Also, detailed studies have revealed the presence in fluid flows of chaotic dynamics with well-defined low-dimensional structure in phase-space.

One area where such ideas have proved especially relevant is Taylor–Couette flow between concentric rotating cylinders. A recent review by Mullin (1993) contains many examples of the significant occurrences of low-dimensional dynamical behaviour in this problem. The basic geometry of the Taylor–Couette system is that of two concentric circular cylinders with a fluid in the separating gap. The fluid is driven round by rotation of the inner cylinder at a constant angular speed. By varying this speed systematically, a series of distinct transitions can be observed. Firstly, there is a mutation from uniform shear flow to steady axisymmetric cells (known as Taylor vortices) as the result of centrifugal instability. These steady cells subsequently become

† Present address: Department of Applied Mathematics and Theoretical Physics, University of Cambridge, Silver Street, Cambridge, CB3 9EW, UK

unstable to travelling waves which propagate around the annular domain. With further increase of the cylinder speed, the travelling waves first develop modulation. Then, with the appearance of other frequency components, a state is reached which is temporally aperiodic but retains the overall spatial structure of the Taylor vortices. A review of some of the sequences which are observed is given by DiPrima & Swinney (1981).

An alternative approach to the problem is to include the height of the annulus as a variable parameter in addition to the speed of the cylinder. It is then possible to follow the loci of these and other critical transitions in parameter space. Such an approach is insightful when allied with the formalism of nonlinear dynamics and bifurcation theory, since it is then possible to identify the origin of apparently complicated behaviour with the interaction between much simpler events.

Despite the success of using ideas from low-dimensional models to understand the behaviour observed in the Taylor–Couette problem, it is not clear that such an approach is appropriate for more general systems in fluid dynamics. This may be attributed to the fact that the Taylor–Couette system embodies a high degree of geometrical symmetry. Typically, the vertical extent of the flow domain is determined by either two stationary or two rotating end-plates. Thus there is mirror symmetry about the horizontal mid-plane of the system, represented formally by a discrete $\mathbb{Z}_2$ symmetry group. More significantly as far as time-dependent flows are concerned, there is continuous azimuthal symmetry around the annular domain. This results in the presence of a continuous $SO(2)$ symmetry group in the problem. Such a condition makes possible the existence of the travelling waves which are observed in the sequence of transitions leading to irregular flow (see Crawford *et al.* 1991 for a fuller discussion of the role of symmetries in bifurcation problems). The fact that most fluid dynamics problems do not have such a well-defined regular state in their solution structures can be attributed to the fact that they rarely possess the degree of symmetry found in the Taylor–Couette problem. Likewise, it is possible that the detailed bifurcation sequences which provide the underlying finite-dimensional mechanisms are not to be found in other flows.

The approach which is adopted in this study consists of modifying the geometry of the Taylor–Couette problem by replacing the outer circular cylinder with one of square cross-section. Thus, there is no longer an axisymmetric domain, but rather one with a discrete $\mathbb{Z}_4$ symmetry azimuthally, and still the $\mathbb{Z}_2$ midplane reflectional symmetry. A sketch of this square variant of the Taylor–Couette system is shown in figure 1(*a*,*b*).

Such a square system has been used in previous experimental studies. Snyder (1968) established that steady cellular flows, similar to Taylor vortex flow, exist in the square system for sufficiently high Reynolds number. Mullin, Lorenzen & Pfister (1983) made a preliminary study of time-dependent flows with $\mathbb{Z}_4$ azimuthal symmetry. They observed that the steady cellular flow becomes unstable to a singly periodic mode as the Reynolds number is increased. However, unlike in the standard Taylor–Couette system, this mode is not a simple travelling wave but is a more complicated motion of the cells. Further increase of the Reynolds number leads to a side-band instability and then to temporally non-periodic flow. Significantly, this final state was observed by Mullin *et al.* to be devoid of any spatial structure. This is in marked contrast to the flow in the standard system, where the cellular structure is found to persist well into the turbulent regime (Smith & Townsend 1982). The first detailed bifurcation study of flows in the square Taylor–Couette system was carried out by Mullin & Lorenzen (1985). They investigated experimentally the mechanism

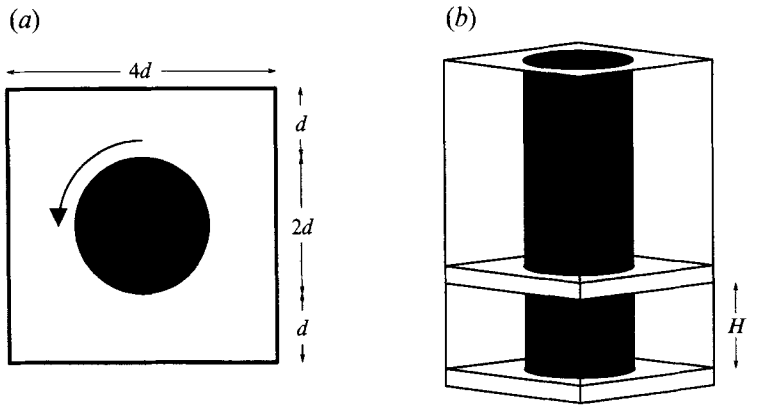

FIGURE 1. Schematic diagram showing the geometry of the square Taylor–Couette system: (*a*) plan view; (*b*) perspective view.

for exchange between the time-independent four-cell and six-cell primary modes. The general exchange mechanism for the case of the standard system, first proposed by Benjamin (1978), is now well understood, and the reader is directed to the review by Cliffe, Kobine & Mullin (1992) for details. Mullin & Lorenzen uncovered a similar mechanism in the square system, involving secondary modes which are disconnected from a primary mode. However, it was found that the exchange procedure was obscured to a certain extent by the presence of time-dependent modes.

In all three of the above studies, the vertical extent of the flow domain was sufficiently large to allow there to be several cells present in the flow. However, it is known from the work of Benjamin & Mullin (1981) on the standard Taylor–Couette system that the solution structure associated with the flow comprising a single cell differs quite substantially from the case of several cells. In particular, it is the case that the single-cell solution remains connected to the primary mode, whereas all other odd-numbered cellular flows are always disconnected solutions.

In this present study, we choose to focus on the single-cell flow which exists in the square Taylor–Couette system. This is done by restricting the vertical extent of the domain to the order of the gap between the two cylinders. The objective is two-fold. Firstly, it is necessary to establish whether the steady-state bifurcation structure for the standard single-cell flow is structurally stable under the change to $\mathbb{Z}_4$ azimuthal symmetry. This being the case, the fact that there is a minimum of multiplicity in the solution set of single-cell flow means that it is an ideal vehicle for investigating detailed bifurcation phenomena which would otherwise be obscured by a plethora of neighbouring solutions. Therefore, secondly, we seek to determine whether any of the low-dimensional dynamic phenomena which are found under conditions of continuous $SO(2)$ azimuthal symmetry can be observed for discrete $\mathbb{Z}_4$ symmetry. Only if this is the case can we begin to be confident in the applicability of ideas from low-dimensional dynamical systems to a wider class of closed-flow problems.

The remainder of this paper proceeds as follows. In § 2, there is a description of the apparatus and measuring techniques which were used in the study. The experimental results for steady single-cell flow are presented in § 3, together with a comparison with similar features in the standard system. The time-dependent flows are introduced in § 4, and this is followed in § 5 by results which show the regular dynamics to be organized by a structure of low-dimensional bifurcations.

More complicated dynamical phenomena are considered in § 6, culminating in the observation of behaviour similar to that of the finite-dimensional Šil'nikov mechanism. Finally, conclusions are drawn in § 7.

2. Experimental details

In this section, a description is given of the apparatus and the measuring techniques which were employed. The outer cylinder of the flow rig was constructed from four uniform glass plates. These were glued together on a milled aluminium former to ensure a precise square cross-section. The interior length of each side was equal to 63.57 ± 0.05 mm. The inner cylinder was machined from solid stainless steel to a uniform diameter of 31.78 ± 0.01 mm. This value was chosen to give a ratio of the diameter to the length of side which is equal to 0.500 ± 0.001.

The vertical extent of the flow domain was defined by the separation between two horizontal end-plates. These were cut from 16 mm thick pieces of PTFE and were made to fit closely to the outer cylinder but with a small amount of clearance at the rotating inner cylinder. The lower block rested on the base of the rig, while the upper block was supported from above by two metal rods on either side of the inner cylinder. The rods extended through the lid of the rig, and allowed the vertical separation to be varied continuously over the range 0–170 mm. The actual value was determined using a precision travelling telescope which measured to an absolute accuracy of 0.02 mm.

The inner cylinder was supported in PTFE bearings, and was rotated by means of a stepping motor connected through a reduction gearbox and a pulley system. The driving mechanism was such that the angular speed was directly proportional to the frequency of the oscillator signal which was supplied to the stepping motor. This frequency had a stability over the course of the experiments which was better than 0.1%.

The flow domain was surrounded along its entire length by a Perspex container. This formed a sealed jacket through which thermally regulated distilled water was pumped at 27.3°C by a Haake temperature controller. The purpose of this was to ensure a constant temperature of the working fluid, and therefore a constant kinematic viscosity. As a further step to this effect, the flow rig was housed in a large cabinet in which the air temperature was held at 27°C using an electric fan heater connected to a mercury switch thermometer. These two thermal controls had the effect of holding the temperature of the working fluid constant to better than 0.02°C during the experiments.

The Reynolds number for this system is defined to be $Re = \omega r d/\nu$, where ω is the angular speed of the inner cylinder, r is the radius of that cylinder, d is the minimum horizontal separation between the inner and outer cylinder and ν is the kinematic viscosity of the fluid. The high geometrical precision of the flow rig and the strict temperature control meant that the relative accuracy of Re was effectively determined only by the stability of the oscillator which supplied the driving mechanism for the inner cylinder.

A second dimensionless parameter is required to characterize the state of the system. This is the aspect ratio Γ, defined as $\Gamma = H/d$. Here, H is the perpendicular distance between the horizontal ends of the flow domain, and d is the minimum gap between the inner and outer cylinders. The value of H has already been stated to have an absolute error of 0.02 mm, and so for the aspect ratios which are typical for these experiments (i.e. $\Gamma \approx 1$), this gives a relative error for Γ of approximately 0.1%.

The fluid which was used in the steady-flow experiments was a 50:50 mixture of distilled water and Glycerol. The kinematic viscosity was measured using a suspended-level viscometer, and was found to have a value of $\nu = 5.90 \pm 0.01$ mm^{2}s^{-1} at the operating temperature of 27.3°C. A small quantity of flow visualization material was added to the fluid at a concentration of approximately 0.01%. The material was Mearlmaid AA natural pearl essence, which is made of tiny anisotropic platelets that are essentially neutrally buoyant in the working fluid. Flow structures were discerned by projecting a thin, vertical sheet of light through the fluid in the narrowest gap between the cylinders. The motion in the illuminated plane was viewed either by eye or through a travelling telescope with a cross-hair eye piece and an accurate Vernier traverse. In our experience, this global view of the flow field is the most useful way of studying critical phenomena in steady flows.

However, when studying time-dependent phenomena, a laser Doppler velocimeter (LDV) was used to obtain quantitative information about the flow dynamics. The output from a 2 mW He-Ne laser was directed into a prism beam-splitter to produce two parallel coplanar beams of equal intensity. These then passed through Bragg cells which shifted the frequency of the light in each beam to give a relative difference in frequency of 100 kHz. The beams were then focused at their point of intersection to define a small measuring volume in the flow. The Doppler-shifted light which was scattered as seeding particles passed through this volume was detected by a photomultiplier. The Doppler frequency was transformed by a phase-locked loop circuit into a voltage which was directly proportional to the radial velocity component. It was important that the choice of measuring position gave dynamical information which was typical of the dynamics of the flow as a whole. Care was always taken to ensure that this was the case, and the actual measuring positions are given when appropriate.

The seeding particles in this case were latex spheres with an average diameter of 6.4 μm. They were distributed uniformly in the fluid by the action of an ultrasonic bath prior to the fluid being poured into the flow rig. For the studies of time-dependent phenomena, silicone oil or mixtures of water and glycerol were used, with viscosities ranging from 2 to 6 mm^{2}s^{-1}at 27.3°C.

3. Bifurcation structure for steady flows

In this section, results are presented of experiments which were carried out to explore the steady bifurcation structure in the square Taylor–Couette system at aspect ratios close to unity. To begin with, changes in the structure of the flow are described qualitatively for increasing values of Γ. This is followed by the results of measurements of the critical parameter values at which bifurcations occur in the two-dimensional parameter space defined by Re and Γ.

3.1. *Bifurcation sequence*

The bifurcation sequence which was observed experimentally is shown qualitatively in figure 2(a–d) for four successively larger values of aspect ratio Γ, with the Reynolds number Re as the bifurcation parameter. The trivial solution branch from which the bifurcating branches emerge corresponds to a two-cell flow that is symmetric about the horizontal midplane of the domain. This is the primary mode for this particular range of aspect ratio.

To begin with, the first effect of increasing Re is that a pitchfork bifurcation to stable single-cell flow is encountered (figure 2a). The solution which arises at this

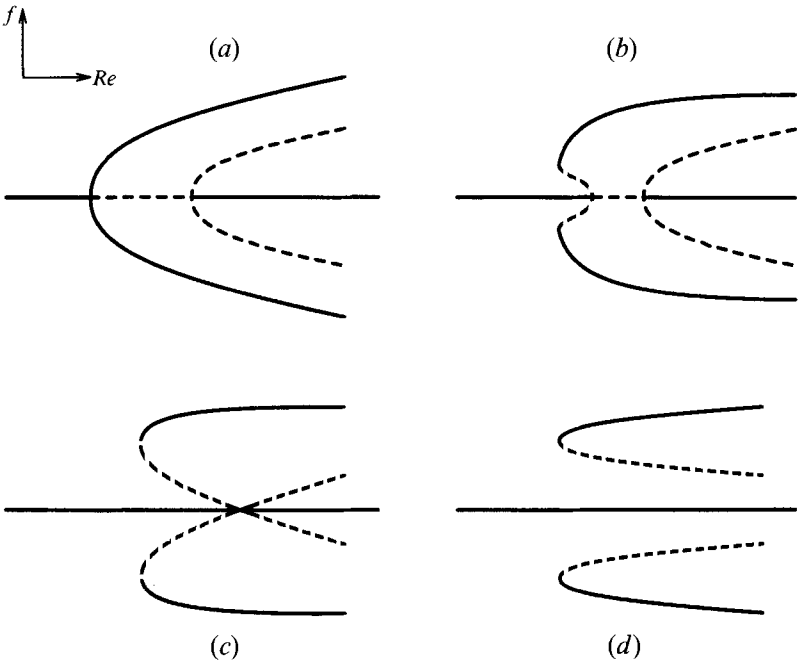

FIGURE 2. Bifurcation sequence for two-cell and single-cell flows in the standard Taylor–Couette system. The trivial branch corresponds to symmetric two-cell flow. The aspect ratio is increasing from (*a*) to (*d*), with the Reynolds number as the bifurcation parameter in each case. Pitchfork bifurcations are shown as symmetric for the sake of clarity, although they are actually asymmetrically disconnected by the presence of unavoidable imperfections.

bifurcation breaks the $\mathbb{Z}_2$ symmetry which is imposed on the flow by the geometrical boundary conditions. In addition, the now unstable symmetric solution branch is restabilized by an unstable pitchfork bifurcation at higher *Re*. As the aspect ratio is increased, these two bifurcation points approach each other. This is accompanied by a change in the first pitchfork from supercritical to subcritical (figure 2*b*). At a critical value of aspect ratio, the two bifurcations coalesce (figure 2*c*). Beyond this point, the two single-cell solutions are disconnected from the primary branch (figure 2*d*). It should be noted that for the sake of clarity all the pitchfork bifurcations in figure 2(*a*–*d*) have been drawn as symmetric. However, in practice the pitchfork bifurcations are encountered in disconnected form due to the small imperfections which are inevitable in a physical system.

This bifurcation sequence is the same as is found for single-cell flow in the standard Taylor–Couette system. It was first proposed by Benjamin & Mullin (1981), who went on to confirm their conjecture with experimental measurements. The same bifurcation mechanism was found subsequently by Cliffe (1983) using numerical techniques which allowed both the stable and the unstable solution branches to be calculated. Part of the bifurcation sequence involving the change in the symmetry-breaking bifurcation from supercritical to subcritical was confirmed experimentally by Aitta, Ahlers & Cannell (1985). Most recently, Pfister *et al.* (1988) carried out experimental and numerical work on two-cell and single-cell flows in the standard Taylor–Couette system, and obtained excellent agreement between the two sets of data.

3.2. *Quantitative results*

In the flow-visualization experiments, the illuminated region of the flow was observed through a travelling telescope with a cross-hair eye piece. In order to measure the critical values of Re associated with symmetry-breaking in the two-cell flow, the horizontal cross-hair was positioned so that it coincided with the midplane of the flow domain. Thus any asymmetry in the flow could be detected as a departure of the line of separation between the two vortices from this horizontal marker.

A practical problem here is that, as has already been stated, the symmetry-breaking bifurcation is disconnected by unavoidable imperfections in the system. There is therefore no critical point at which symmetry is broken, but rather a continuous transition from symmetric to asymmetric flow. This indeterminacy in measurement can be overcome by focusing instead on the turning point which marks the lower stability limit of the disconnected solution branch. In the experiments, the Reynolds number was increased suddenly to give the single-cell flow which corresponded to the disconnected branch of the pitchfork bifurcation. Once this had been achieved, Re was gradually reduced until the lower limit of stability of the disconnected solution was encountered. Although the collapse was a subtle event, it could nevertheless be detected by an irreversible change in the direction of the vertical flow component at a representative point on the horizontal cross-hair. The procedure was repeated several times in order to obtain successively more accurate measurements of the critical Reynolds number, which was ultimately limited in accuracy by the stability of the oscillator controlling the speed of the inner cylinder (see § 2).

The procedure for measuring the critical point for the secondary symmetry-breaking bifurcation involved first establishing the stable two-cell flow at higher Reynolds number. This was done by sudden increase of Re to successively larger values until a stable two-cell flow was seen to persist. The Reynolds number was then decreased, and a similar refinement technique to that described above was used to locate the critical value of Re. Sudden starts were also used for the disconnected single-cell solutions until the stable single-cell flow was established, and then the Reynolds number was decreased to locate the lower limit of stability. In both these cases, there was no requirement to locate the symmetry plane since the transitions were of a much more definite nature than for the case of the primary symmetry-breaking bifurcation.

The limits of hysteresis in the primary pitchfork bifurcation were also measured. The presence of the disconnection means that hysteresis is only exhibited in the primary solution branch, so the experiments could proceed without the requirement first to locate a disconnected solution. The method again involved placing the horizontal cross-wire of the telescope eye piece coincident with the symmetry plane of the annulus. The Reynolds number was then gradually increased from zero until the separating line between the two vortices suddenly departed from the horizontal cross-wire. This critical value corresponded to the upper turning point of the hysteresis region. Similarly, with sufficient decrease of Re, the flow reverted catastrophically back to being symmetric about the midplane. It was possible with small changes in Re to locate the limits of this hysteresis to the relative accuracy of the oscillator controlling the speed of the inner cylinder.

A factor which had to be taken into account when carrying out all the measurements was the rate at which transient flow decayed when changes were made to the Reynolds number. It was observed that this time varied significantly depending on whether or not the system was close to more than one bifurcation point. For the majority of measurements, the decay time was found to be of the order of the timescale

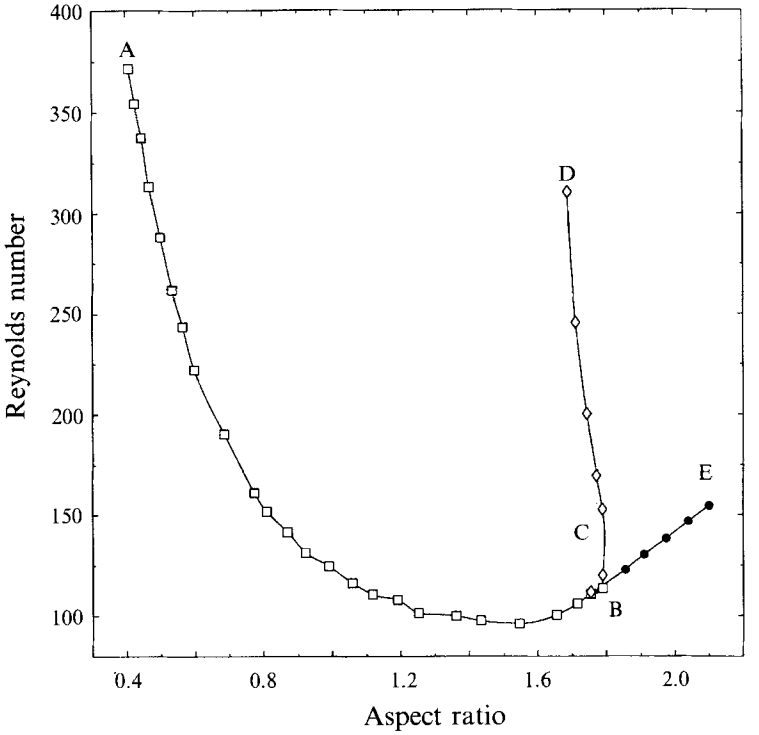

FIGURE 3. Experimentally determined bifurcation set in the square system: AB (□), primary pitchfork bifurcation to single-cell flow; CD(◇), secondary pitchfork bifurcation which restabilizes two-cell flow; BE(•), limit point which marks lower stability limit of disconnected single-cell flow. Lines are drawn purely to guide the eye.

$\tau = d/(\nu\omega)^{1/2}$ which is obtained from a simple dimensional analysis. However, for measurements taken when the system was close to the coalescence of the two pitchfork bifurcations, transient times of up to 4000τ were recorded. The effect is to cause the system to remain for a long time in the vicinity of the unstable symmetric solution before collapsing to the final asymmetric state. Under these conditions, it was only possible to achieve repeatable results by allowing times in excess of 4000τ between the small changes of Re which were required to locate bifurcation points accurately.

The above considerations are consistent with results which were obtained by Pfister *et al.* (1988) for the decay of transients in the standard Taylor–Couette system. Time constants were measured experimentally and numerically by Pfister *et al.* for several values of the Reynolds number in the interval separating the two pitchfork bifurcations for the sequence equivalent to that shown in figure 2(*b*). It was found that the time constant has an approximately parabolic variation across the interval, with a minimum value halfway between the two bifurcation points.

The loci of the three different types of bifurcation which have been measured in the present study are shown in figure 3. The plot is of the two-dimensional parameter space defined by aspect ratio Γ and Reynolds number Re. The results show that the bifurcation sequence found in the standard system by Benjamin & Mullin also exists for the variant with a square outer boundary. The locus AB marks the path of the primary symmetry-breaking bifurcation resulting in single-cell flow. The locus CD is a similar path for the subcritical pitchfork bifurcation that restabilizes the symmetric two-cell flow. The lines are not continued beyond points A and D respectively because

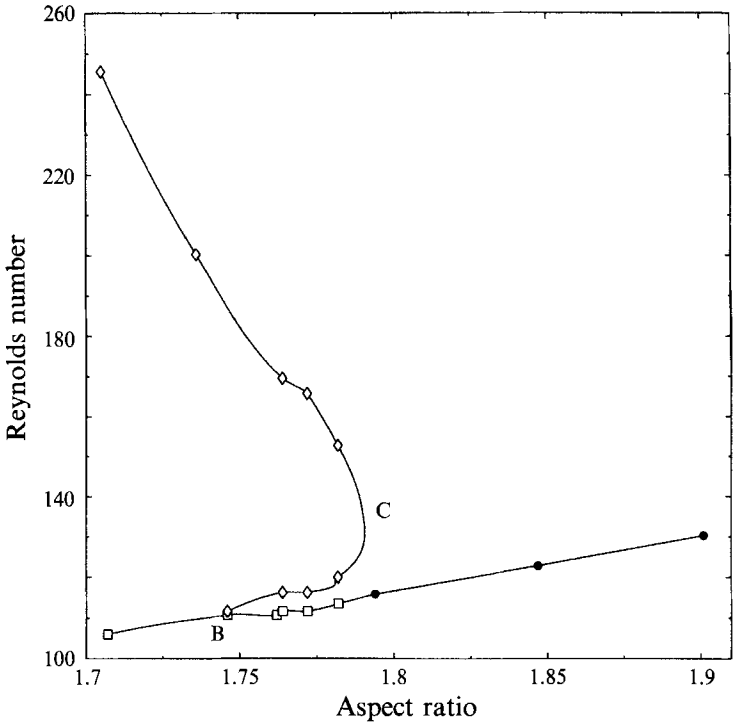

FIGURE 4. Expanded view of parameter space around point C in figure 3 showing hysteresis in the primary symmetry-breaking bifurcation.

it was at these parameter values that time-dependent effects were encountered. As Γ is increased, the lines AB and CD of critical points converge. The primary pitchfork bifurcation goes through a quartic point and develops hysteresis, just as was found by Benjamin & Mullin. This results in the splitting of the symmetry-breaking locus at point B in figure 3. The two subcritical points connect at point C, resulting in the full stabilization of the symmetric solution branch. The disconnected single-cell flow has a lower limit of stability represented by the limit point whose locus is the line BE. For consistency, these results were measured using just one of the two possible single cells. The locus of limit points certainly continues beyond the point E, but measurements were terminated at this point since there was no further qualitative change in this solution.

An expanded view of the parameter space around point C is presented in figure 4, where the development of hysteresis and the subsequent disconnection of the single-cell solution can be seen more clearly. It should be noted that the range over which the hysteresis is present is only 0.7 mm in these experiments. Nevertheless, the details of the solution set over this range are essential to the understanding of the overall flow behaviour.

3.3. *Comparison with the standard system*

We have already seen in § 3.1 that there is strong qualitative similarity between the steady-state bifurcation sequences found at small aspect ratios in Taylor–Couette systems with circular and square outer cylinders. However, it is also possible to compare some quantitative aspects of the results obtained from the two systems.

The symmetry-breaking bifurcation set for the standard system with radius ratio

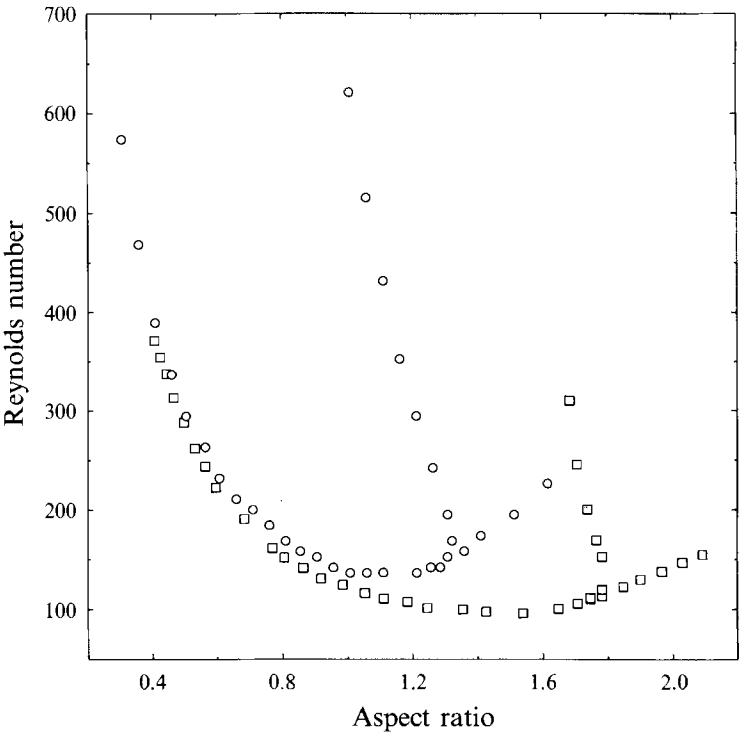

FIGURE 5. Overlay of the results from the standard (○) and square (□) systems with radius ratios of $\eta = 0.5$ based on minimum separating gaps. It can be seen that the two lines of primary pitchfork bifurcations converge for $\Gamma < 1$.

$\eta = 0.5$ has been determined experimentally and numerically by Pfister *et al.* (1988). It is therefore possible to make a direct quantitative comparison of the results of measurements of bifurcation points, as long as the defining lengthscale is taken as the gap (the minimum gap in the case of the square system) between inner and outer cylinders.

An overlay of the results of the present study with those of Pfister *et al.* is shown in figure 5. The important feature to note is the strong quantitative similarity in the loci of the primary symmetry-breaking bifurcations for aspect ratios $\Gamma < 1$. This convergence phenomenon can be understood physically by considering the nature of the three-dimensional flow that is driven by the inner cylinder at small aspect ratios. The frictional effect on the flow of the stationary ends means that the only significant motion is restricted to fluid close to the rotating cylinder. Thus, prior to the symmetry-breaking bifurcation, the two-cell flow is confined principally to a region whose radial extent is approximately equal to the vertical separation between the end-plates. This symmetric flow undergoes bifurcation to single-cell flow where the single Taylor cell occupies the same region as was previously determined by the two-cell flow.

A consequence of this restriction of the cellular flow to the proximity of the inner cylinder is that the exact details of the shape of the outer boundary become less significant as the aspect ratio is decreased below the value of one. Thus it is possible to understand how two systems, one with a circular outer boundary and the other with a square outer boundary, can be practically indistinguishable through experimental

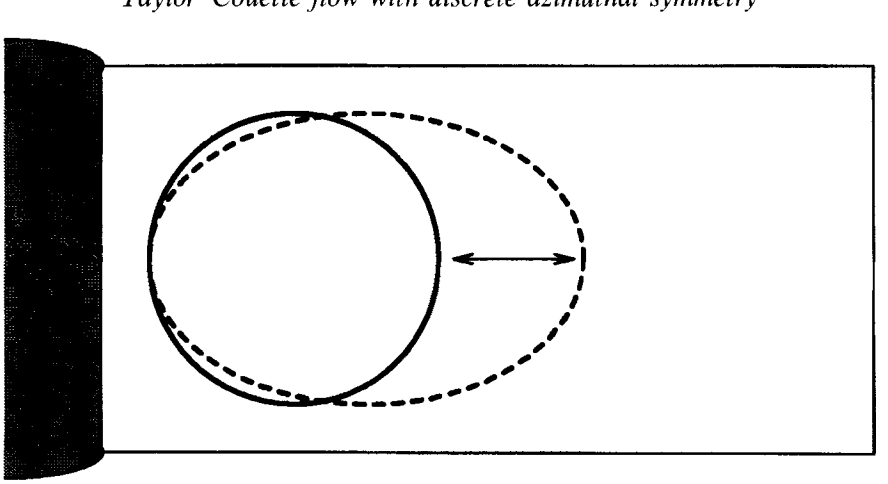

FIGURE 6. Oscillatory behaviour of single-cell flow in the square Taylor–Couette system for $\Gamma < 1$. The previously steady, circular-shaped cell now oscillates between circular and oblate cross-sections.

measurement of the critical Reynolds number for symmetry-breaking at small aspect ratios.

4. Characteristics of time-dependent flows

It has been established in § 3 that the solution structure for steady single-cell flow is organized in qualitatively the same manner as for the corresponding flow in the standard Taylor–Couette system. We now proceed to an investigation of the time-dependent single-cell flow in the square system.

Before looking in detail at the time-dependent bifurcation structure which exists in this problem, it is instructive to consider certain qualitative and quantitative aspects of the time-dependent single-cell flow. It was found that two different types of oscillatory behaviour are possible for single-cell flow in the square Taylor–Couette system. These are described below, together with data which show the onset of time-dependence to be the result of Hopf bifurcations. The section is concluded with a comparison with time-dependent single-cell flow in the standard Taylor–Couette system.

4.1. *General characteristics*

The first type of behaviour was encountered for aspect ratios less than one. It was observed in § 3 that the steady single-cell flow for $\Gamma < 1$ only has significant motion close to the inner cylinder in a region with radial extent approximately equal to the vertical separation between the end-plates. When the Reynolds number was increased sufficiently, this steady configuration was observed to develop a time-dependent aspect. The region of secondary circulation which is used to define the Taylor cell then oscillated in a predominantly radial direction between a circular and an oblate shape. This behaviour is illustrated in figure 6. We define the dimensionless frequency of oscillation as $\Omega = 2\pi f/\omega_c$, where f is the dimensional frequency and ω_c is the angular speed of the rotating inner cylinder. A value of $\Omega = 0.3$ was recorded at the onset of this oscillation at all values of Γ at which it was observed.

The second type of oscillatory behaviour occurred typically for $\Gamma > 1$. A cycle begins with the appearance of a small vortex at the inner cylinder approximately halfway between the horizontal ends (figure 7*a*). The circulation of this new vortex

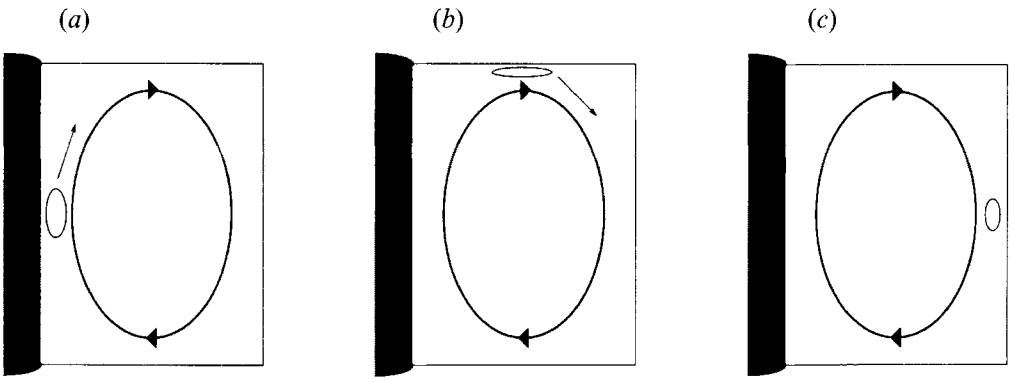

FIGURE 7. Oscillatory behaviour of single-cell flow in the square Taylor–Couette system for $\Gamma > 1$: (*a*) a small vortex grows between the main cell and the rotating inner cylinder; (*b*) the vortex moves round with the prevailing secondary flow, reaching maximum strength as it moves close to the stationary end-plate; (*c*) the vortex dissipates upon reaching the stationary outer cylinder. This cycle repeats with a regular period.

is in the opposite sense to that of the main Taylor cell. Once formed, the vortex moves round with the main flow causing a small local deformation of the cell outline. The strength of the peripheral vortex reaches a maximum as it is swept radially outward along the end-plate (figure 7*b*). Finally the vortex dissipates at the stationary outer boundary of the flow domain (figure 7*c*). The dimensionless frequency of the oscillation at onset was measured as $\Omega \approx 0.2$ over the majority of the aspect ratio range in which it occurred. However, it will be seen in §6 that the dynamic nature of flows for $\Gamma > 1$ can be highly dependent on both the aspect ratio and the Reynolds number.

4.2. *Identification of simple Hopf bifurcations*

The simple Hopf bifurcation is the most common finite-dimensional mechanism for the loss of stability of a steady solution to a singly periodic solution with variation of a control parameter μ. There are two characteristic properties which hold local to a simple Hopf bifurcation at $\mu = \mu_c$. Firstly, the amplitude of the oscillation grows as $(\mu - \mu_c)^{1/2}$ for $\mu > \mu_c$. Secondly, the frequency of oscillation is independent of μ. The latter property is a consequence of a complex-conjugate pair of eigenvalues crossing the imaginary axis transversely as μ is varied through μ_c. There is, however, a generalized Hopf bifurcation where the crossing is not transverse, and in that case the frequency of the oscillatory solution does depend on the bifurcation parameter. For details see Golubitsky & Langford (1981).

The LDV system was used to measure the amplitude and frequency of the oscillation in the radial velocity component at a fixed point in the flow domain. This point was always located radially midway between the inner and outer cylinders where the gap between the two was narrowest. However, the axial position could be varied, and it is convenient to define a dimensionless linear axial coordinate $h \in [0, 1]$ for the measuring volume. Here, $h = 0$ corresponds to the end-plate next to which there is inward radial flow, while $h = 1$ corresponds to the other end-plate.

Measurements were made of the two types of time-dependent flow at $h = 0.5$, one set at $\Gamma = 0.5$ and the other at $\Gamma = 1.5$. The results are shown in figure 8(*a–d*). The solid lines in figures 8(*a*) and 8(*c*) are least-squares fits of the form $A = k(Re - Re_c)^{1/2}$, where A is the amplitude of the oscillation in arbitrary units and k is the fitting

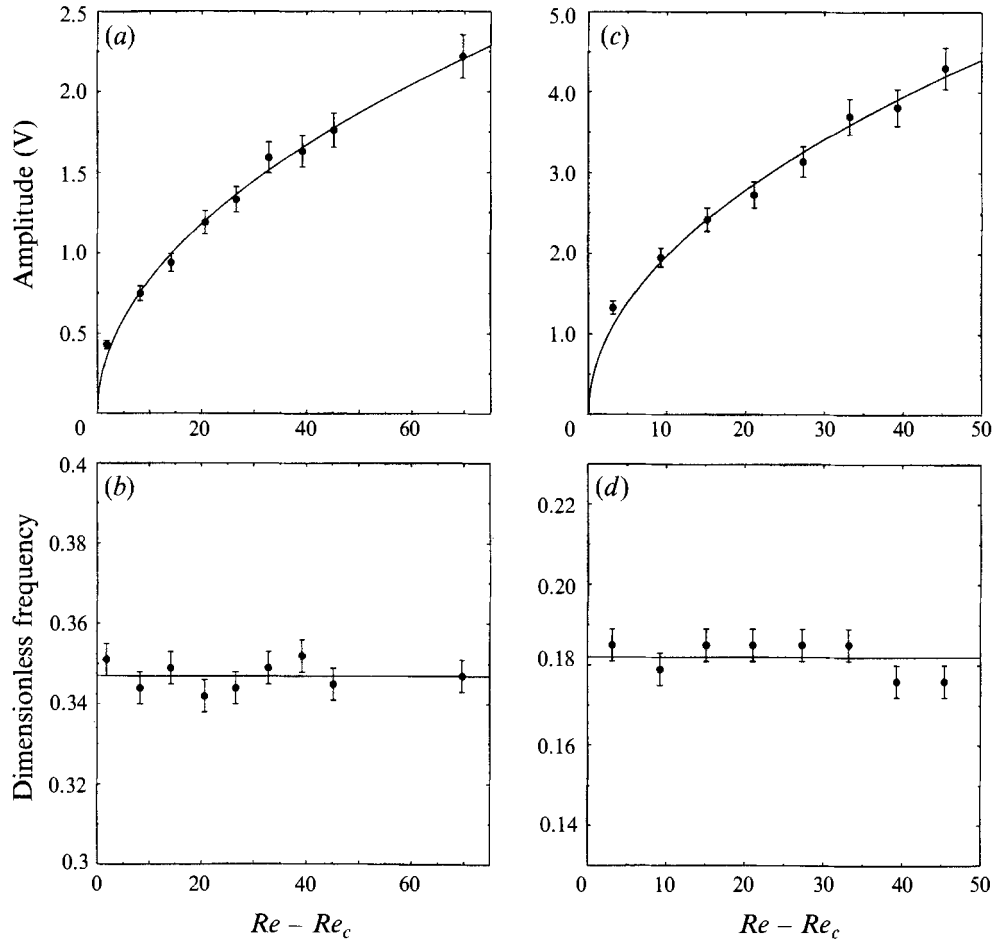

FIGURE 8. Results of LDV measurements which show characteristic features of a Hopf bifurcation. (*a*) Amplitude and (*b*) dimensionless frequency for $\Gamma = 0.5, Re_c = 587.24$. (*c*) Amplitude and (*d*) dimensionless frequency for $\Gamma = 1.5, Re_c = 452.76$.

parameter. In both cases, the fit is within the limits of experimental error. The results for the dimensionless frequencies of the two oscillations are shown in figures 8(*b*) and 8(*d*). The horizontal lines were obtained from linear regression performed on each set of data. They show that both dimensionless frequencies remain constant for Reynolds numbers in a range of approximately 10% of the critical value.

Thus we see that the two characteristics of a simple Hopf bifurcation are present in the onset of the modes which are illustrated in figures 6 and 7(*a–c*). This has been shown in each case for a fixed value of aspect ratio. Results will be presented in § 5 of the effect of varying the aspect ratio on the critical Reynolds numbers for the two Hopf bifurcations.

4.3. *Temporal wavenumbers*

In addition to observing the nature of the oscillations in the profile of the single cells, the structure of the time-dependent flow around the annulus was also determined using flow visualization techniques. This was achieved by measuring differences in phase between planes of cross-section at different azimuthal positions. However,

because of the discrete symmetric nature of the flow domain it is necessary to restrict the concept of a wavelength to that of temporal rather than spatial periods. Thus we identify the azimuthal positions at which the local maxima of the oscillation occur simultaneously, and determine from this a temporal wavenumber k. The results for the class of oscillation represented by figure 6 indicate a wavenumber $k = 2$, while those for the type in figure 7(a–c) gave $k = 3$.

4.4. *Comparison with the standard system*

An experimental study of the dynamics of single Taylor vortex flow in the standard Taylor–Couette system has been carried out by Lensch (1988). The radius ratio η was equal to 0.5, and the flow was driven by rotation of the inner cylinder alone. The height of the annulus was set by the position of two stationary horizontal end-plates. Aspect ratios which were studied by Lensch ranged from $\Gamma = 0.4$ to $\Gamma = 1.3$.

The qualitative nature of time-dependent single-cell flows in the standard system was found to be the same as has been described above for the square configuration. For aspect ratios less than one, the cell profile oscillates between circular and oblate in a predominantly radial direction. The oscillation for Γ greater than one consists of the periodic formation of small vortices at the inner cylinder which then move round the outside of the main cell and are destroyed at the outer boundary.

A quantitative comparison can be achieved by considering the respective dimensionless frequencies of each mode in the two systems. For aspect ratios less than one, Lensch reports a value of $\Omega = 0.3$ in the standard system. This is the same as the value for the corresponding mode in the square system. However, the agreement does not persist for $\Gamma > 1$. A value of $\Omega = 0.06$ is quoted by Lensch, whereas the modified system gives $\Omega \approx 0.2$. A possible explanation for the different values of dimensionless frequency for one range of aspect ratio and the agreement for another comes from the distinct nature of the two time-dependent modes. The oscillating single cell for $\Gamma < 1$ in both the standard and modified systems is effectively localized to a region of the flow domain close to the inner cylinder. It is therefore possible that this type of flow is insensitive to the exact details of the outer wall geometry. However, the oscillation for $\Gamma > 1$ has a strong effect on the whole flow field. Hence it is not surprising that a change in the shape of the outer boundary might produce a change in a quantitative aspect of this flow.

A second quantitative comparison is possible in terms of the wavenumbers of the flows. We saw above that subject to certain qualifications about the use of a wavenumber in an annulus without continuous rotational symmetry, the modes for $\Gamma < 1$ and $\Gamma > 1$ can be labelled with wavenumbers $k = 2$ and $k = 3$ respectively. However, Lensch reports a value of $k = 3$ for $\Gamma < 1$ and $k = 2$ for $\Gamma > 1$ in the standard system. These values have been confirmed by subsequent experiments (H. Röpcke, private communication 1992). This is the reverse of the case for the square system. The reasons for the reversal are not understood at present, and this result clearly shows the limitation of arguments based simply on the qualitative nature of the single-cell flows.

5. Elementary bifurcation structure for time-dependent flows

We have seen in § 4 that there are two qualitatively different time-dependent modes which can arise from the steady single-cell flow in the square Taylor–Couette system. These modes are the result of simple Hopf bifurcations on the asymmetric solution branches of the symmetry-breaking bifurcation from two-cell to single-cell flow.

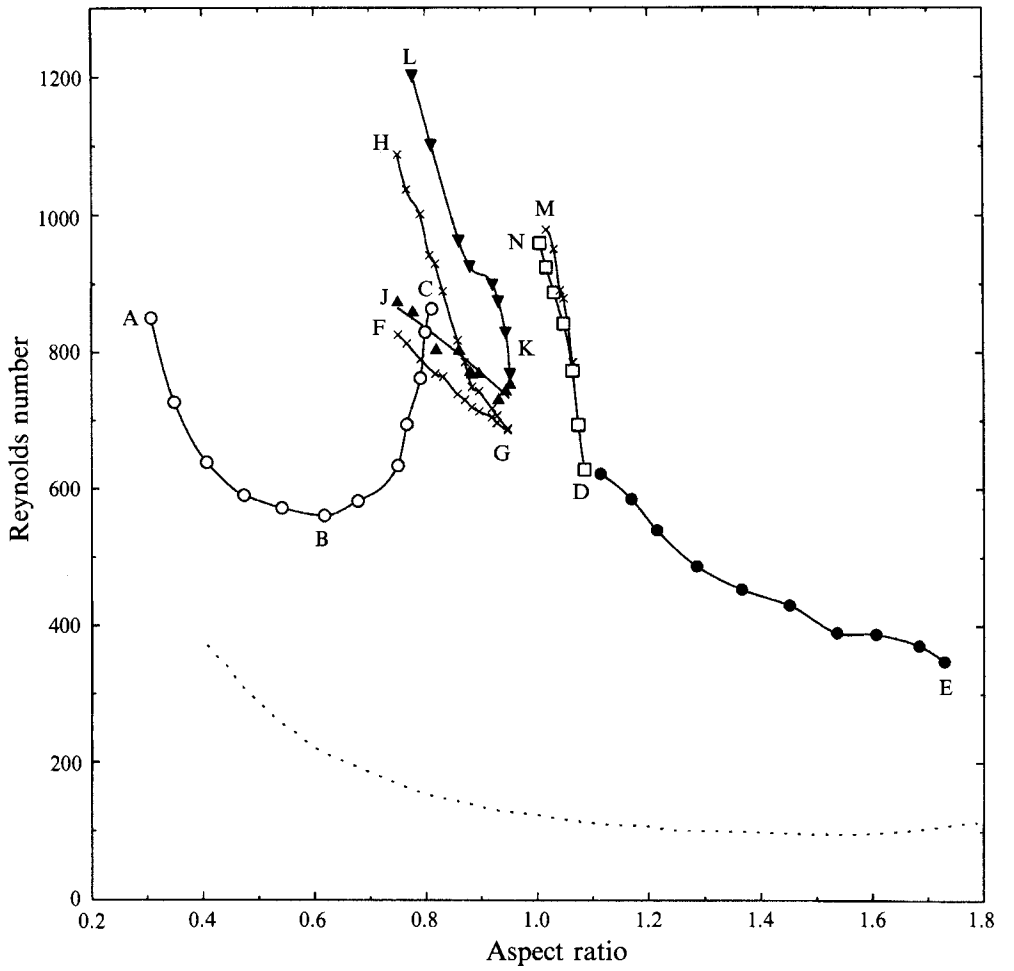

FIGURE 9. Parameter-space diagram showing experimentally determined lines of bifurcations. Dotted line is locus of symmetry-breaking bifurcations to steady single-cell flow. ABC (○) and DE (•): Hopf bifurcations. FGH (×): limits of hysteresis between circular and extended cell. JKL: Hopf (▲)-inverse Hopf (▼) isola. MD (×): limit points. ND (□): homoclinic bifurcations.

Careful experimental investigation has revealed a detailed but self-consistent dynamic bifurcation structure in this problem. The individual elements of this structure are shown together in the bifurcation set of figure 9, and are discussed separately below. This is followed by a comparison with the bifurcation structure which is known to exist in the standard system.

5.1. *Bifurcation structure for* $\Gamma < 1$

The lines ABC and DE in figure 9 are the loci of Hopf bifurcations leading to the $k = 2$ and $k = 3$ modes respectively. The dotted line marks the path of the primary symmetry-breaking bifurcation from two-cell to single-cell steady flow. We will refer to the aspect ratio which corresponds to a point P as Γ_P. In this notation, Γ_A was the smallest value at which the LDV system could be operated, while Γ_E was the chosen limit beyond which the locus was not followed.

The locus ABC of Hopf bifurcations was found to terminate at point C as the result of a hysteretic transition involving a novel form of single-cell flow. It was observed in

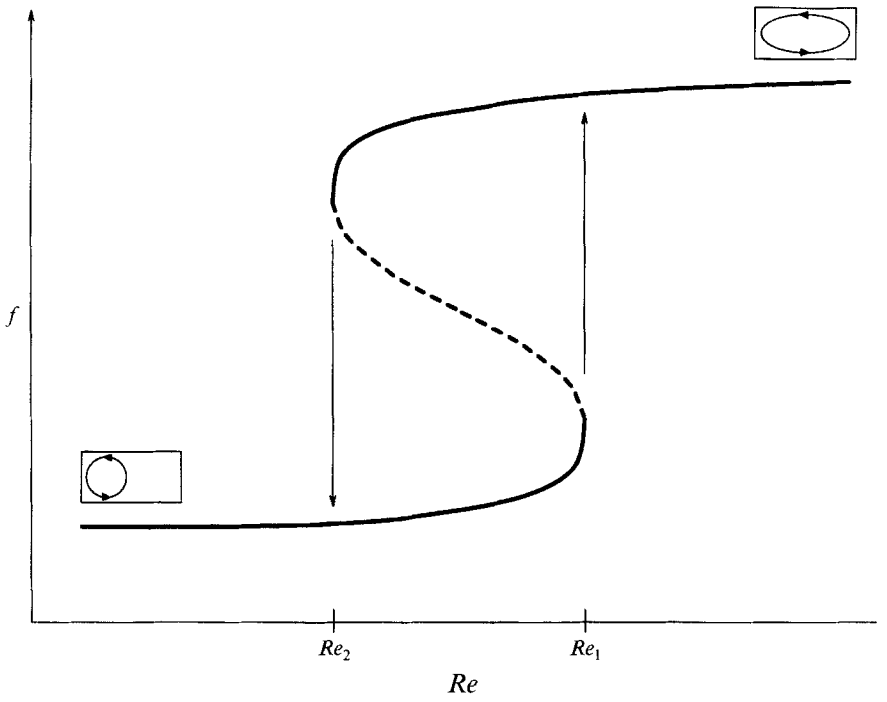

FIGURE 10. Bifurcation diagram for the transition between circular and extended forms of steady single-cell flow. Solid lines represent stable solutions, while the dashed line indicates an unstable solution. The quantity f is any linear functional which discriminates between the two types of flow. Experimentally, this was taken as the radial velocity component at a point in the domain.

§ 3 that the steady single cell which first develops at the symmetry-breaking bifurcation for $\Gamma < 1$ has an approximately circular cross-section and is limited in the radial direction to a region close to the rotating inner cylinder. However, the new single-cell flow is different in that it extends to fill the full radial extent of the flow domain. A possible bifurcation sequence which describes the exchange between the two flows is shown in figure 10. This has the form of two limit points which are connected by an unstable solution branch. The circular cell persists with increase of Re until the bifurcation at Re_1 is encountered. The flow then changes catastrophically to the extended form of the single cell. The reverse transition occurs upon decreasing Re to the point Re_2, where Re_2 is less than Re_1. Qualitatively identical bifurcation sequences were found to exist on both the asymmetric branches of the pitchfork bifurcation from two-cell to single-cell flow. Measurements were always made on the connected branch for the sake of consistency.

Results of LDV measurements of the hysteretic transition over a range of aspect ratio are shown in figure 9. The locus FGH of critical points forms a standard hysteresis cusp in parameter space. For aspect ratios between Γ_C and Γ_G, the steady circular single-cell flow persists until the line CG is crossed from below. The flow then evolves to the extended form of the single cell, and remains so until the line FG is crossed from above. The upper and lower limits of the hysteresis region coincide at the point G, where $\Gamma_G \approx 0.95$. This convergence can be understood in terms of the progressive lack of distinction between the two types of single-cell flow as the aspect

ratio is increased towards one. It should be noted that no such hysteresis transition has been observed in the single-cell flow in the standard Taylor–Couette system.

Thus there is a codimension-2 bifurcation formed near the point C, where a Hopf bifurcation and a limit point occur simultaneously. However, it proved impossible to locate the codimension-2 bifurcation point exactly because of the sensitivity of the system to small changes in the control parameters in the region where the two lines of bifurcations are close together.

For aspect ratios less than Γ_C, the effect of increasing the Reynolds number beyond the Hopf bifurcation at BC is that a limit point is encountered. The $k = 2$ oscillatory form of the circular cell persists with unchanged dimensionless frequency until a critical value of Re is reached, at which point there is a catastrophic collapse to the extended single-cell flow. The experimentally determined locus CH of these limit points is shown in figure 9. Once achieved, the extended single-cell flow does not revert to the circular form until the line FG of limit points is crossed from above.

A complicating factor in the hysteretic transition from both the steady and the time-dependent circular cell to the extended cell is that the latter flow is typically encountered in a time-dependent form. The bifurcation diagram was explored at a fixed value of the aspect ratio. This revealed the existence of two Hopf bifurcations on the upper solution branch corresponding to the extended single cell. The time-dependent solution exists as an isola on the solution branch, with inward-facing Hopf bifurcations at each end. Thus the steady extended cell can be restabilized from its time-dependent form by either increasing or decreasing the Reynolds number.

Measurements of the critical Reynolds numbers of the two Hopf bifurcations were made over a range of aspect ratio. The results are shown in figure 9 as the locus JKL, and thus the point K is an isola formation point in parameter space. The extended single-cell flow is time-dependent for all parameter values within the region defined by the line JKL. The proximity of the locus JK of Hopf bifurcations to the locus FG of limit points, which mark respectively the upper and lower limits of stability of the extended cell, shows that there is only a narrow range of parameter values at which the steady flow can be observed experimentally at the lower end of the time-dependent isola.

The dimensionless frequency of the oscillation in the extended single-cell flow was found to have a value of $\Omega = 0.04$ over the range of aspect ratio which was considered. This is in contrast to the value of $\Omega = 0.3$ which is associated with the time-dependent circular cell. Observation of the spatial structure of the oscillating extended cell using flow visualization revealed a cycle which was reminiscent of the time-dependent flow found in general for aspect ratios greater than one. There was the periodic formation of a small vortex between the inner cylinder and the main cell. This vortex then moved around the outside of the extended cell, but now in the opposite direction to the main circulation. This is in contrast to the time-dependent sequence shown in figure 7(a–c) for $\Gamma > 1$, where the peripheral vortex moves in the same direction as the circulation.

5.2. *Bifurcation structure for* $\Gamma > 1$

For aspect ratios just less than Γ_D, observations were made of homoclinic phenomena. A homoclinic orbit in phase space is one which asymptotically approaches the same fixed point as time $t \to \pm\infty$. In the context of a dynamical system, this is when the period of an oscillatory solution becomes infinite with variation of one or more control parameters. In an experimental situation, obviously no oscillation can be observed which has infinite period. Rather, a system is said to be approaching a

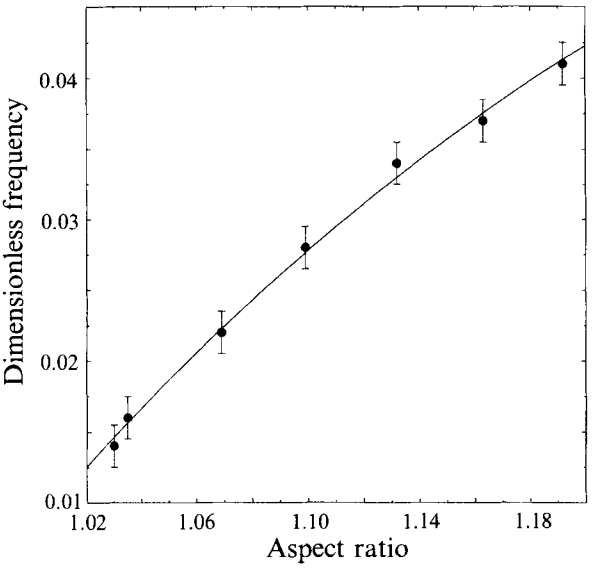

FIGURE 11. Variation of the dimensionless frequency of oscillatory single-cell flow with aspect ratio as the locus DN of homoclinic bifurcations (figure 9) is approached. The Reynolds number is held fixed at $Re = 900$.

state of homoclinicity when the period of an oscillation is far in excess of the typical timescale of the problem. A careful investigation of such flow phenomena was made for aspect ratios just less than Γ_D.

The line MD in figure 9 is a locus of sudden transitions from steady to time-dependent flow with increase of Reynolds number. The oscillation appeared with non-zero amplitude as the line MD was crossed from below. Once established, the oscillation was found to persist with decrease of Re to a value which was slightly lower than the value associated with the critical point for the onset of the oscillation. The approach towards the lower limit of stability was accompanied by a continuous drop in the value of the dimensionless frequency, indicating that the oscillation was becoming homoclinic. The locus of homoclinic bifurcations back to steady flow is shown in figure 9 as the line ND. It should be noted that these two lines of bifurcations exist in close proximity in parameter space. Careful experimental procedure was therefore required in order to make measurements of the respective critical points. Nevertheless, it proved impossible to resolve the small amount of hysteresis which almost certainly exists close to the point D.

The loci MD and ND both rise steeply in the given representation of parameter space. The critical points were therefore much more easily investigated by fixing the Reynolds number and varying the aspect ratio. The variation of the dimensionless frequency as the locus ND of homoclinic bifurcations was approached in this way is shown in figure 11 for Reynolds number $Re = 900$. Here we can see clearly the continuous decrease in dimensionless frequency over a narrow range of control parameter which is characteristic of an impending homoclinic bifurcation.

5.3. *Comparison with the standard system*

Results for the bifurcation structure of time-dependent single-cell flow in the standard Taylor–Couette system have been presented by Lensch (1988) and Pfister, Schulz & Lensch (1991). In both cases, experiments were carried out in a system with radius

ratio $\eta = 0.5$, and with the outer cylinder and the end-plates all stationary. We will restrict ourselves here to a qualitative consideration of the results, and refer to the appropriate references for the full details.

For aspect ratios less than one, there is a locus of Hopf bifurcations to the $k = 3$ mode (the wavenumbers being the reverse of the case in the square system) which is qualitatively similar to that found in the square system. This locus is also terminated by the upper limit of a hysteresis region, but the hysteresis is now that of a subcritical Hopf bifurcation to the $k = 2$ mode. At larger values of aspect ratio, the bifurcation structure is dominated by homoclinic phenomena. The loci of critical points in parameter space are different from those obtained from the square system, and involve eventually a type-II intermittent transition to chaos.

Thus we see again the tendency for similar behaviour in the standard and square systems when the aspect ratio is less than one, and any significant flow is confined near the inner cylinder. However, as the aspect ratio is increased and the oscillation influences more of the flow domain, the effect of the shape of the outer boundary becomes more pronounced. There is then a divergence in behaviour. Nevertheless, it remains the case that the dynamics in both systems are described in the context of low-dimensional dynamical systems. Thus while the precise details of the time-dependent behaviour may change in going from continuous to discrete azimuthal symmetry, the fundamental nature of the dynamics does not.

6. More complicated dynamical phenomena

The results which were presented in §5 show that, just as was the case in §3 for steady flows, the time-dependent single-cell flows in the square Taylor–Couette system are organized in terms of simple bifurcations which are well understood from the study of nonlinear dynamical systems. We proceed now to consider results which show a more complicated dynamical flow behaviour that is similar to a low-dimensional mechanism found in a Taylor–Couette system with continuous $SO(2)$ azimuthal symmetry.

The results as shown in figure 9 suggest that the effect of varying the aspect ratio such that the locus DE is followed would give rise to a monotonic change in the critical Reynolds number associated with the Hopf bifurcation. However, a plot of the dimensionless frequency of the oscillation at its onset versus aspect ratio indicates that the behaviour is more complicated than this. It can be seen in figure 12 that for aspect ratios greater than $\Gamma = 1.235$, the dimensionless frequencies are of the order $\Omega = 0.2$. However, there appears to be a discontinuous change in the value of Ω at $\Gamma = 1.235$. For aspect ratios below this value, the frequency drops suddenly to the order of $\Omega = 0.01$. The presence of such a change requires explanation, and it will be shown that the answer is to be found in the detailed bifurcation structure which manifests itself at values of the aspect ratio around $\Gamma = 1.235$.

6.1. *Qualitative considerations*

Flow visualization experiments revealed qualitatively different behaviour in the time-dependent flows on either side of the discontinuous change in dimensionless frequency. For the higher-frequency mode ($\Gamma > 1.235$), the cycle is the same as that illustrated in figure 7(*a–c*). Small vortices are formed at the inner cylinder and move round in the same direction as the prevailing secondary flow. However, for the lower-frequency mode ($\Gamma < 1.235$), the difference is that the peripheral vortices now move in the opposite direction. This is the same behaviour that was found for the time-dependent

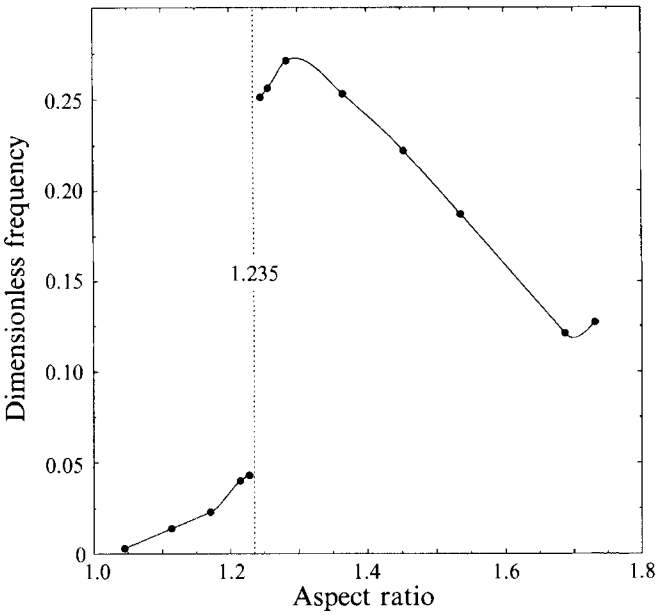

FIGURE 12. Plot of dimensionless frequency at the onset of oscillation along the line DE of Hopf bifurcations in figure 9.

form of the *extended* single-cell flow for $\Gamma < 1$, in the region of parameter space contained by the locus JKL in figure 9. Thus it is reasonable to conclude that the Hopf bifurcation which is encountered for aspect ratios just below $\Gamma = 1.235$ is the same Hopf bifurcation which is found at the values of Γ associated with the extended single cell.

6.2. *Detailed bifurcation structure*

We now wish to change from considering the relatively wide range of parameter space which is shown in figure 9, to focusing our attention on a narrow section centred on $\Gamma = 1.24$. A magnified parameter-space diagram is shown in figure 13 containing features of a more detailed nature which were uncovered as a consequence of refined experiments. These new features are discussed individually below.

It was found that there is in fact a multiplicity of time-dependent single-cell flows, with both the modes being observed at the same set of control parameters. We will adopt the nomenclature introduced by Benjamin (1978) to describe the relative characteristics of the two modes. A mode which results from the quasi-static variation of only one control parameter through one or other of the Hopf bifurcations will be referred to as the primary mode. The other mode, which is necessarily realized by variation of both parameters or by a sudden change in one of them, will be referred to as the secondary mode. Thus for $\Gamma > 1.235$, the primary mode is the higher-frequency oscillatory flow and the secondary mode is the lower-frequency flow. For $\Gamma < 1.235$, the roles of the two modes are reversed.

A characteristic feature of a secondary mode is that it is terminated by a turning point and thus has a lower limit of stability. This is indeed found to be the case for both the higher- and lower-frequency secondary modes in the present study. The secondary modes collapse catastrophically at a critical set of control parameters, and the system reverts to the dynamics of the appropriate primary mode. The lower

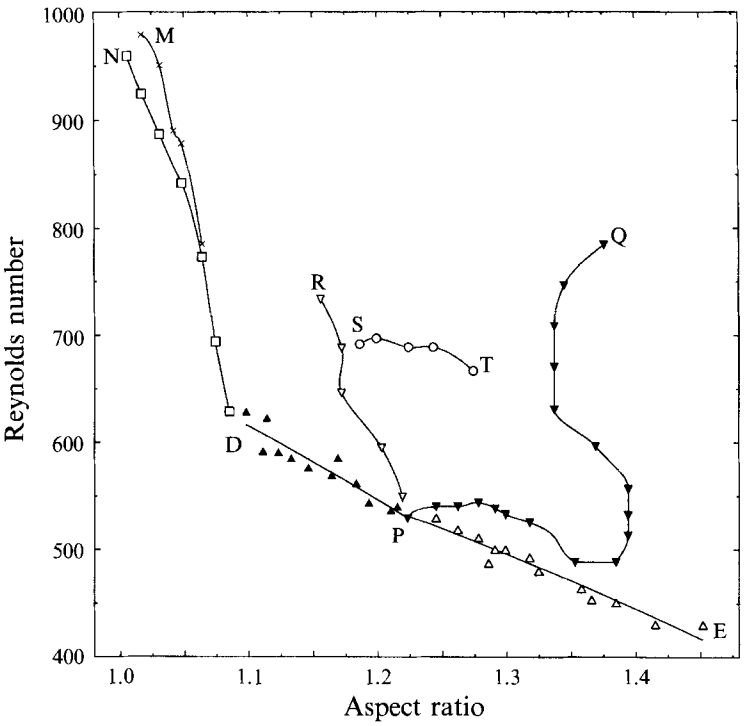

FIGURE 13. Magnified view of parameter space about the apparent discontinuous change in dimensionless frequency. Some symbols have been changed from those used in figure 9. PE (△): Hopf bifurcation leading to higher-frequency mode. PR (▽): stability limit of higher-frequency mode. PD (▲): Hopf bifurcation leading to lower-frequency mode. PQ (▼): stability limit of lower-frequency mode. ST (○): secondary Hopf bifurcation

stability limits of the two secondary modes were measured experimentally over a range of aspect ratio using the LDV system. The results are shown in figure 13. The locus PQ represents the lower stability limit of the lower-frequency mode, while the locus PR is that of the higher-frequency mode. Thus it can be seen that what appeared initially in figure 9 as a single line of critical points is in fact two different lines which intersect at $\Gamma \approx 1.235$.

The effect of increasing the Reynolds number was investigated with regard to the higher-frequency mode which arises at the locus PE of Hopf bifurcations. The result was that a secondary Hopf bifurcation was encountered. This is a bifurcation from a singly periodic mode to a doubly periodic mode, which is an oscillation comprising two distinct frequency components. Time-series consist of the original oscillation with a regular modulation of the amplitude envelope. An example of this behaviour is shown in figure 14.

The variation of the critical Reynolds number for the secondary Hopf bifurcation was investigated over a range of aspect ratio. The results are shown in figure 13 as the locus ST, where the point T was the chosen upper limit on the range of measurement. The significant feature of these results is that they indicate an intersection of the line of secondary Hopf bifurcations with the locus RP of periodic folds which marks the lower stability limit of the singly periodic mode. Thus there is a probable codimension-2 bifurcation in parameter space, close to the point S, where a periodic fold and a secondary Hopf bifurcation occur simultaneously. The exact position

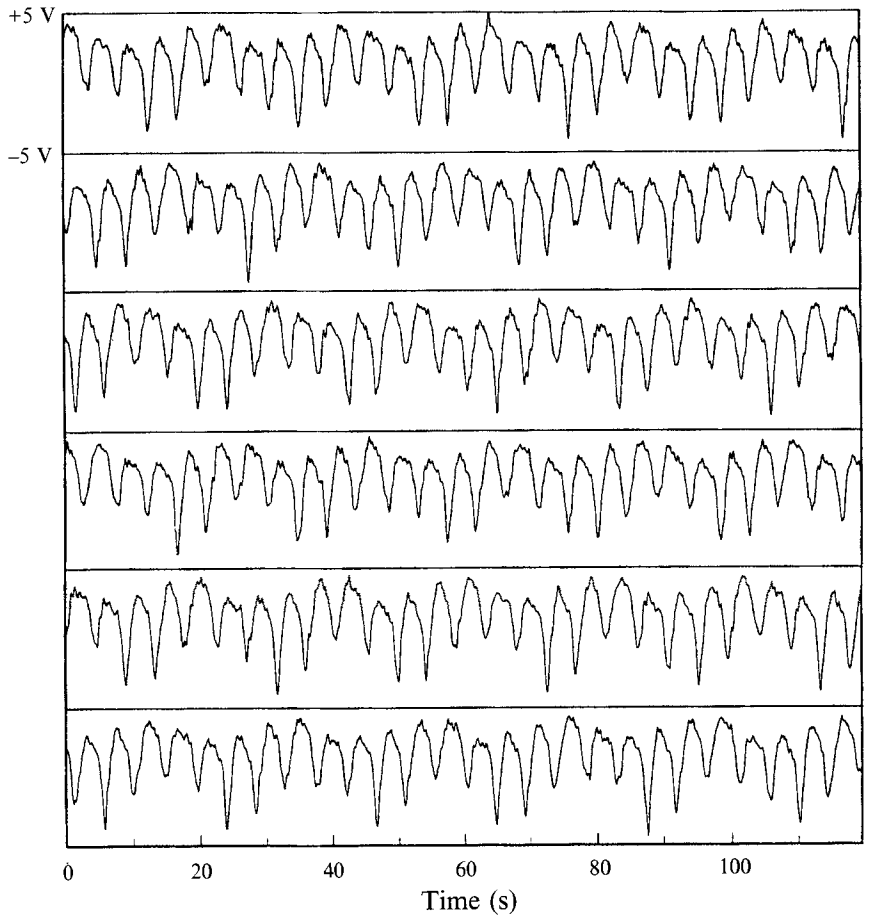

FIGURE 14. Example of modulated oscillatory behaviour as the result of a secondary Hopf bifurcation. Recorded at measuring position $h = 0.53$ with $\Gamma = 1.28$, $Re = 677.24$.

of this bifurcation could not be determined experimentally because of the extreme sensitivity of the system to changes in the control parameters as the locus RP of folds is approached. The point S represents the closest position which was attainable with the present system, whose main limitation was the degree to which the aspect ratio could be varied without causing an excessive perturbation to the flow. Nevertheless, the experimental results suggest that the locus ST intersects the locus RP. This is further attested to by the fact that the section of the locus RP above the point S marks the lower stability limit of the doubly periodic mode. The modulated oscillation was found to persist with decrease of Γ until this upper section of the line RP was crossed. The flow then collapsed catastrophically to the singly periodic lower-frequency mode which originates at the Hopf bifurcation indicated by the locus DP in figure 13.

6.3. *Dynamical behaviour of the Šil'nikov type*

The final stage of this study involved increasing the Reynolds number from the secondary Hopf bifurcation which occurs at the line ST in figure 13. The aim was to explore further into the nonlinear regime and test if the low-dimensional nature of the flow dynamics would persist or be replaced by more complicated effects.

The effect of increasing Re was investigated for a fixed value of aspect ratio,

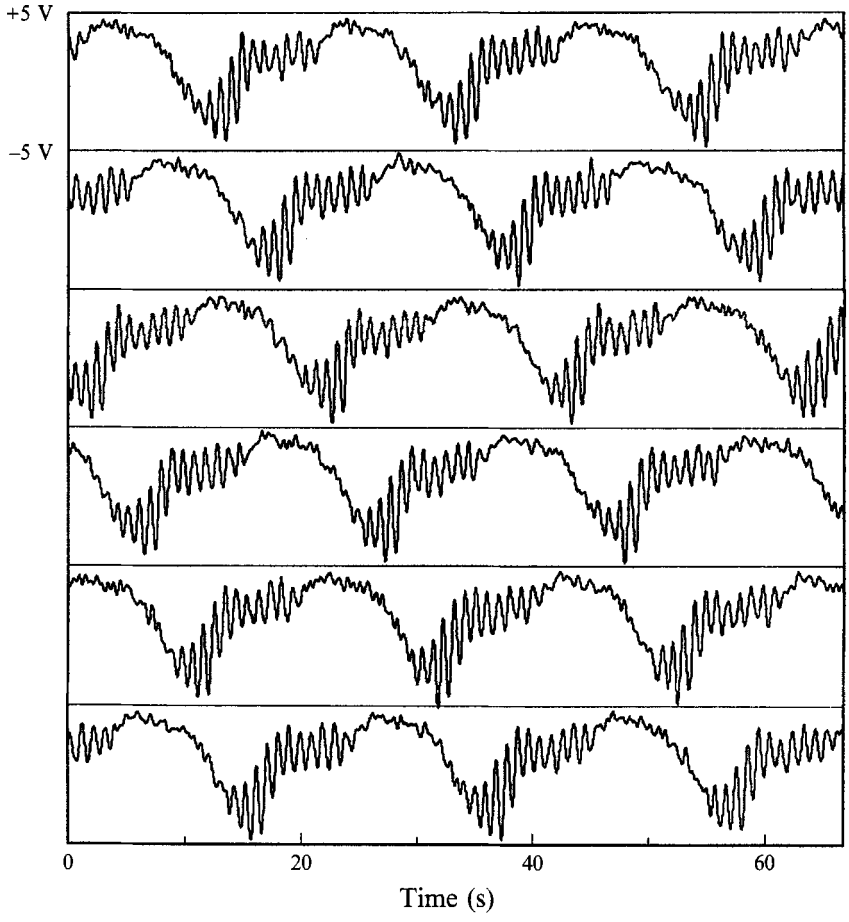

FIGURE 15. Section of a time-series recorded at measuring position $h = 0.79$ with $\Gamma = 1.25$, $Re = 766.07$. The mode comprises a low-frequency oscillation which is punctuated regularly by high-frequency intervals.

$\Gamma = 1.25$. The flow remained qualitatively unchanged in the modulated oscillatory state until $Re = 766$. At that point, the previously regular modulated behaviour developed an irregular aspect. After a transient time corresponding to approximately 2400 revolutions of the inner cylinder, the flow was observed to change to a new dynamic state. This is illustrated by the time-series which is shown in figure 15. It is clear that there are two elements to this particular flow. There is a lower-frequency oscillation together with a higher-frequency component which is visible at intervals throughout the time-series. This behaviour was found to persist for at least 10^5 rotations of the inner cylinder. In addition, it was possible to establish such a flow repeatedly by starting the system from rest and gradually increasing the Reynolds number to the present value. Thus it was concluded that the motion being observed was a stable and persistent feature.

The time-series of which a section is shown in figure 15 was used to obtain a reconstructed phase-space representation of the dynamics. This was performed computationally using the method of delays combined with singular value decomposition (SVD) as developed originally by Broomhead & King (1986). The result is a set of trajectories in phase space, known as a phase portrait, along which time

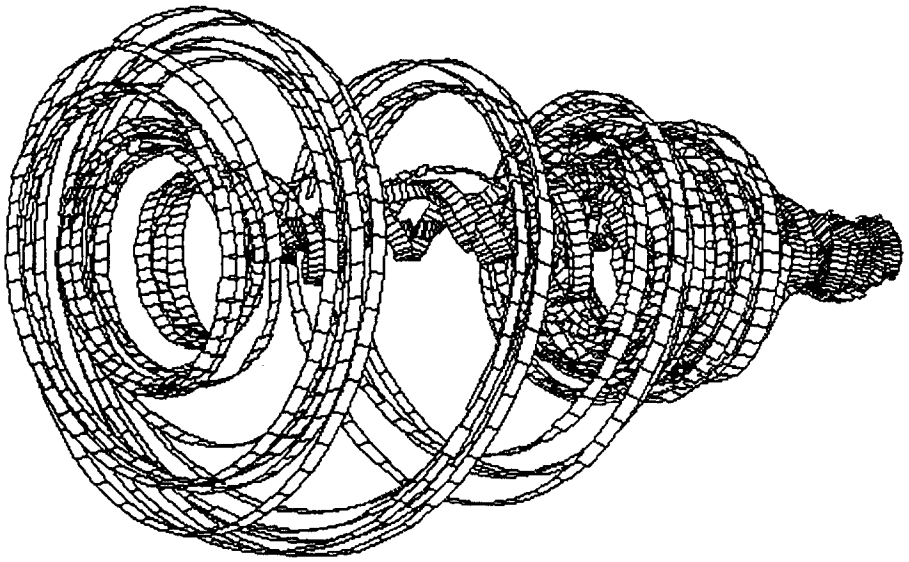

FIGURE 16. Phase-space reconstruction using the time-series of which a section is shown in figure 15. Trajectories are drawn as ribbons in order to depict the three-dimensional structure of the object.

is a parameter. The phase portrait which was obtained in this case is shown in figure 16. The motion takes place on a distorted torus which has a narrow central core. The core begins at the far end of the torus, where the high concentration of points indicates that the system spends a relatively long period of time in this region. Such behaviour suggests the presence of a weakly unstable fixed point, with an unstable direction along the core of the torus. At the near end, the motion appears to become unstable to perturbations in a plane approximately perpendicular to the core. Individual trajectories can be seen to spiral outward initially, and then wind back towards the far end of the object. A feature of this return mechanism is the high concentration of orbits just before the trajectories return to the weakly unstable fixed point. There is the suggestion of a weakly unstable limit cycle around the core which causes the system to spend a disproportionate length of time in its vicinity.

The significance of the above observations is two-fold. Firstly, a similar type of dynamical behaviour was observed experimentally by Mullin & Price (1989) while investigating a different Taylor–Couette problem. They considered flow between two concentric circular cylinders where the inner cylinder and the end-plates rotated together. The symmetries were thus a continuous $SO(2)$ group around the annulus and a discrete $\mathbb{Z}_2$ mirror symmetry about the midplane of the annular gap. The particular mode which was studied was a time-dependent four-cell flow which had undergone a symmetry-breaking bifurcation with respect to the $\mathbb{Z}_2$ group. Time-series presented by Mullin & Price show a higher-frequency component which appears in short bursts, separated by relatively long quiescent phases. The phase portrait, which was reconstructed using the same techniques which were employed in the present study, shows the same type of structure as in figure 16. There is a central core of trajectories with a spiraling motion around the outside. More recently, similar dynamical behaviour has been observed experimentally in a system where only one of the two end-plates rotates with the inner cylinder, thereby removing the $\mathbb{Z}_2$ midplane symmetry (V. Heinrich, private communication 1993).

The second point of significance is that the present results and those obtained by Mullin & Price are highly reminiscent of behaviour exhibited by a nonlinear finite-dimensional dynamical system first studied by Šil'nikov (1965). A detailed description of this system is given by Guckenheimer & Holmes (1986), and we consider here only the essential elements. It involves a saddle point in three-dimensional phase space where the stable manifold is a spiral on a sheet and the unstable manifold is a line perpendicular to the sheet. Trajectories spiral inwards and are eventually ejected out of the plane, only to return along the stable manifold. This system is capable of supporting homoclinic orbits, which correspond to closed trajectories that asymptote to the saddle point as $t \rightarrow \pm\infty$. A bifurcation parameter controls the proximity of the system to a homoclinic orbit. A feature of varying this parameter is that forward and inverse cascades of period-doubling bifurcations are encountered, as shown by Glendinning & Sparrow (1984).

The oscillatory flows in the square system and in the system with $SO(2)$ symmetry both occur with periods which are long in comparison to the basic timescale of the problem. This may be taken as an indication of each system being near a state of homoclinicity. In addition, Mullin & Price showed that a small change in one of the control parameters (they varied the aspect ratio by 0.14%) results in a transition from regular dynamics to an irregular regime where the higher-frequency bursts arrive at varying intervals. Although in the present case the dynamics were only observed in a regular state, it was also found that the mode existed in only a small region of parameter space. Therefore it is possible that the system was not sufficiently close to homoclinicity to allow a transition to irregular behaviour to be observed, and that a greater degree of control over the governing parameters is needed to resolve events which occur close to the stability limits of this particular flow.

7. Conclusions

In recent years, the standard Taylor–Couette system with continuous $SO(2)$ azimuthal symmetry has become a powerful tool for investigating the role which low-dimensional dynamics have to play in explaining the onset of disorder in the motion of a fluid. With the present study, it is hoped that a step has been taken towards generalizing this approach to a wider class of fluid flow problems. Specifically, the results which have been presented here may be taken as a body of evidence in support of the structural stability of low-dimensional dynamics under the change from continuous $SO(2)$ symmetry to discrete $\mathbb{Z}_4$ symmetry azimuthally.

The philosophy has been to restrict the extent of the flow domain in the axial direction, thereby minimizing the multiplicity which is inherent in the solution set. Typically the flow consisted of only a single Taylor cell. Such a flow has been studied previously in the standard Taylor–Couette system, and so can be taken as a source of comparison when the outer circular cylinder is replaced by one with square cross-section. Previous studies of flows in this square configuration have been carried out at larger aspect ratios. However, the results which were obtained in those studies suffered from complicating factors which almost certainly arose as a result of the increased multiplicity of flows. By studying single-cell flow, it has proved possible to avoid those extra complications and hence investigate detailed phenomena which are essential to the problem.

A feature of previous research into the Taylor–Couette problem has been the extent to which progress has been made through a combination of careful experimentation and computation. In the latter case, the problem is formulated in terms

of axisymmetric flow, and numerical bifurcation techniques such as path following and centre-manifold reduction are used to construct efficient computational schemes. The present results now raise the possibility of performing similar calculations for the square Taylor–Couette system. Although the flows here are three-dimensional as a result of the discrete azimuthal symmetry, we have seen that both steady and time-dependent flows are organized by simple bifurcation structures. Thus it ought to be possible to extend existing numerical bifurcation techniques and obtain results which could be compared with the experimental data that have been presented.

The observation of dynamics in the square Taylor–Couette system which are suggestive of the finite-dimensional Šil'nikov mechanism is considered to be most important. Similar behaviour has been observed by Mullin & Price (1989) in the standard system. These results were viewed as providing strong evidence for a connection between the Navier–Stokes equations for fluid motion and properties of finite-dimensional dynamical systems. However, this was qualified by the fact that the continuous azimuthal symmetry makes for a highly non-generic fluid flow problem. Now we have such behaviour apparently persisting in a system with discrete azimuthal symmetry. Thus we may begin to look upon finite-dimensional systems such as the Šil'nikov mechanism as being more robust and wide-spread in fluid dynamics than was thought up to now.

The authors wish to express their sincere thanks to Mr K. Long for his technical assistance throughout the course of the experimental work. This research was funded by the SERC (UK) through the Nonlinear Initiative and through a postgraduate studentship (J.J.K.).

REFERENCES

AITTA, A., AHLERS, G. & CANNELL, D. S. 1985 Tricritical phenomena in rotating Couette–Taylor flow. *Phys. Rev. Lett.* **54**, 673–676.

BENJAMIN, T. B. 1978 Bifurcation phenomena in steady flows of a viscous liquid. 1. Theory 2. Experiments. *Proc. R. Soc. Lond.* A **359**, 1–43.

BENJAMIN, T. B. & MULLIN, T. 1981 Anomalous modes in the Taylor experiment. *Proc. R. Soc. Lond.* A **377**, 221–249.

BROOMHEAD, D. S. & KING, G. P. 1986 Extracting qualitative dynamics from experimental data. *Physica* **20**D, 217–236.

CLIFFE, K. A. 1983 Numerical calculations of two-cell and single-cell Taylor flows. *J. Fluid Mech.* **135**, 219–233.

CLIFFE, K. A., KOBINE, J. J. & MULLIN, T. 1992 The role of anomalous modes in Taylor–Couette flow. *Proc. R. Soc. Lond.* A **439**, 341–357.

CRAWFORD, J. D., GOLUBITSKY, M., GOMES, M. G. M., KNOBLOCH, E. & STEWART, I. N. 1991 Boundary conditions as symmetry constraints. In *Singularity Theory and its Applications: Warwick 1989, Part II* (ed. R. M. Roberts & I. N. Stewart). Lecture Notes in Mathematics, vol. 1463. Springer.

DIPRIMA, R. C. & SWINNEY, H. L. 1981 Instabilities and transition in flow between concentric rotating cylinders. In *Hydrodynamic Instabilities and the Transition to Turbulence* (ed. H. L. Swinney & J. P. Gollub). *Topics in Applied Physics*, vol. 45. Springer.

GLENDINNING, P. & SPARROW, C. 1984 Local and global behaviour near homoclinic orbits. *J. Statist. Phys.* **43**, 479–488.

GOLUBITSKY, M. & LANGFORD, W. F. 1981 Classification and unfoldings of degenerate Hopf bifurcations. *J. Diff. Eqns* **41**, 375–415.

GUCKENHEIMER, J. & HOLMES, P. 1986 *Nonlinear Oscillations, Dynamical Systems and Bifurcations of Vector Fields*, 2nd edition. Springer.

LENSCH, B. 1988 Über die Dynamik der Einwirbelströmung im Taylor–Zylinder. Diplomarbeit, University of Kiel, Germany.

MULLIN, T. 1993 Chaos in fluid dynamics. In *The Nature of Chaos* (ed. T. Mullin). Oxford University Press.

MULLIN, T. & LORENZEN, A. 1985 Bifurcation phenomena in flows between a rotating circular cylinder and a stationary square outer cylinder. *J. Fluid Mech.* **157**, 289–303.

MULLIN, T., LORENZEN, A. & PFISTER, G. 1983 Transition to turbulence in a non-standard rotating flow. *Phys. Lett.* A **96**, 236–238.

MULLIN, T. & PRICE, T. J. 1989 An experimental observation of chaos arising from the interaction of steady and time-dependent flows. *Nature* **340**, 294–296.

PFISTER, G., SCHMIDT, H., CLIFFE, K. A. & MULLIN, T. 1988 Bifurcation phenomena in Taylor–Couette flow in a very short annulus. *J. Fluid Mech.* **191**, 1–18.

PFISTER, G., SCHULZ, A. & LENSCH, B. 1991 Bifurcations and a route to chaos of an one-vortex-state in Taylor–Couette flow. *Euro. J. Mech.* B/*Fluids* **10**, 247–252.

ŠIL'NIKOV, L. P. 1965 A case of the existence of a denumerable set of periodic motions. *Sov. Math. Dokl.* **6**, 163–166.

SMITH, G. P. & TOWNSEND, A. A. 1982 Turbulent Couette flow between concentric cylinders at large Taylor numbers. *J. Fluid Mech.* **123**, 187–217.

SNYDER, H. A. 1968 Experiments on rotating flows between noncircular cylinders. *Phys. Fluids* **11**, 1606–1611.